Title

Modified wideband three-dimensional late gadolinium enhancement MRI for patients with implantable cardiac devices

Journal

Magnetic Resonance in Medicine, 75(2)

ISSN

0740-3194

Authors

Rashid, Shams
Rapacchi, Stanislas
Shivkumar, Kalyanam
et al.

Publication Date

2016-02-01

DOI

10.1002/mrm.25601

Peer reviewed

HHS Public Access

Author manuscript

Magn Reson Med. Author manuscript; available in PMC 2016 February 01.

Published in final edited form as:

Magn Reson Med. 2016 February ; 75(2): 572–584. doi:10.1002/mrm.25601.

Modified Wideband Three-Dimensional Late Gadolinium Enhancement MRI for Patients with Implantable Cardiac Devices

Shams Rashid[1], **Stanislas Rapacchi**[1], **Kalyanam Shivkumar**[1,2], **Adam Plotnik**[1], **J. Paul Finn**[1,3], and **Peng Hu**[1,3,*]

[1]Department of Radiological Sciences, David Geffen School of Medicine, University of California, Los Angeles, California, USA

[2]UCLA Cardiac Arrhythmia Center, David Geffen School of Medicine, University of California, Los Angeles, California, USA

[3]Biomedical Physics Inter-Departmental Graduate Program, University of California, Los Angeles, California, USA

Abstract

Purpose—To study the effects of cardiac devices on three-dimensional (3D) late gadolinium enhancement (LGE) MRI and to develop a 3D LGE protocol for implantable cardioverter defibrillator (ICD) patients with reduced image artifacts.

Theory and Methods—The 3D LGE sequence was modified by implementing a wideband inversion pulse, which reduces hyperintensity artifacts, and by increasing bandwidth of the excitation pulse. The modified wideband 3D LGE sequence was tested in phantoms and evaluated in six volunteers and five patients with ICDs.

Results—Phantom and in vivo studies results demonstrated extended signal void and ripple artifacts in 3D LGE that were associated with ICDs. The reason for these artifacts was slab profile distortion and the subsequent aliasing in the slice-encoding direction. The modified wideband 3D LGE provided significantly reduced ripple artifacts than 3D LGE with wideband inversion only. Comparison of 3D and 2D LGE images demonstrated improved spatial resolution of the heart using 3D LGE.

Conclusion—Increased bandwidth of the inversion and excitation pulses can significantly reduce image artifacts associated with ICDs. Our modified wideband 3D LGE protocol can be readily used for imaging patients with ICDs given appropriate safety guidelines are followed.

Keywords

Three dimensional late gadolinium enhancement; delayed enhancement; implantable cardiac devices; implantable cardioverter defibrillator; wideband inversion; hyperintensity artifact; metal artifact reduction

[*]Correspondence to: Peng Hu, Ph.D., Department of Radiological Sciences, 300 UCLA Medical Plaza Suite B119, Los Angeles, CA 90095., penghu@mednet.ucla.edu.

INTRODUCTION

Late gadolinium enhancement (LGE) cardiac MRI is the clinical gold standard for noninvasive assessment of myocardial viability, and is widely used for characterization of focal myocardial fibrosis. Recently, LGE MRI has been playing an increasingly important role in guiding catheter ablation of ventricular tachycardia (VT) because the assessment of scar transmurality, size and location provided by LGE MRI enables accurate identification of the arrhythmogenic substrate and ablation target. However, in the past two decades, there has been a dramatic increase in the prevalence of implanted cardiac devices, such as pacemakers and implantable cardioverter defibrillators (ICDs), for a wide variety of indications. As of 2009, approximately 397,000 pacemakers and 116,000 ICDs were implanted in patients in the United States (1). Up to 75% of the patients with these devices will have an indication for one or more cardiac MRI exams during their lifetime (2). The presence of these devices presents two issues for cardiac MRI: safety and image artifacts. The safety aspect has been extensively studied in the past decade and it has been shown that cardiac MRI can be safely performed at 1.5 Tesla (T) in patients with implanted cardiac devices, provided their rhythm is not device dependent and appropriate guidelines are followed (3–7). The image artifacts are caused mainly by the metallic device generator, which induces strong off-resonance field perturbations within the myocardium. This is particularly problematic for LGE MRI where spurious myocardial hyperintensity results from insufficient spin inversion, which in turn is due to inadequate spectral bandwidth of the nonselective adiabatic inversion recovery (IR) pulses (8,9). These hyperintensity artifacts can mask regions of scar tissue or other late enhancement, severely compromising the diagnostic value of LGE MRI, as this can lead to false negative or false positive diagnoses. Recent studies have shown that these hyperintensity artifacts can be eliminated by using a wideband IR pulse in the LGE sequence (8,9). This modification has been shown to be quite robust in a two-center study for eliminating hyperintensity artifacts (10). Despite these new developments, the current wideband LGE is a two-dimensional (2D) multislice sequence, which limits its achievable signal-to-noise ratio (SNR) and spatial resolution, especially the 2D slice thickness, which is typically 6–8 mm. This limitation can be particularly problematic for studying the correlation between myocardial scar structure provided by LGE MRI and electroanatomical mapping data generated during catheter ablation of cardiac arrhythmias (11–14). High resolution LGE images are feasible using a 3D LGE sequence. However, there have not been any prior studies exploring the feasibility of 3D LGE imaging under the influence of strong off-resonance imposed by cardiac devices; a population where high resolution imaging of scar may be crucial.

Hyperintensity artifacts in LGE images can be considered to fall under the general category of metal-induced artifacts, which has been extensively studied in the literature. Numerous techniques have been proposed for metal artifact reduction in MRI, with varying degrees of success. Multispectral MRI techniques, such as multi-acquisition- variable-resonance image combination (MAVRIC) (15,16), where the off-resonance induced by metallic implants are countered by imaging at multiple resonance frequencies, and combining the resultant images to produce a composite artifact free image, is a promising method for 3D imaging. Another technique, slice encoding for metal artifact correction (SEMAC) (17,18), where the metal-

induced off-resonance is countered by a combination of view angle tilting (VAT) (19,20) and phase encoding in the z-direction, together with an appropriate reconstruction scheme, has been successfully applied in musculoskeletal imaging applications. Recently, a hybrid approach that combines MAVRIC and SEMAC has been proposed (21).

In this report, we present a modified wideband 3D LGE MRI protocol that can readily be used for imaging patients with implantable cardiac devices. This sequence produces LGE images with higher resolution than the current 2D wideband LGE sequences. In addition to the use of wideband IR pulses, we demonstrate that the strong off-resonance of ICDs can produce two additional artifacts in 3D LGE images that do not appear in 2D LGE, and we present a method to substantially reduce these artifacts without requiring additional scan time. Our modified wideband 3D LGE sequence was tested on phantoms and healthy volunteers, and evaluated in patients with previously implanted ICDs.

THEORY

Description of Wideband Inversion Pulse

Hyperintensity artifacts, arising from off-resonance due to the presence of cardiac implantable devices, can be eliminated in LGE by using a wideband inversion pulse; this has been described in detail in prior publications (8,9). The typical inversion pulse used in the LGE sequence in our MRI systems is a nonselective hyperbolic secant (HS) adiabatic pulse of duration 10.24 ms. Adiabatic pulses are generally preferred for inversion recovery processes due to their relative insensitivity to the B1 field, and HS pulses are popular because they have relatively homogeneous, flat inversion efficiency across their spectral bandwidth (22). The HS pulse is composed of the following amplitude and frequency modulation functions (23):

$$A(t)=A_0\mathrm{sech}\beta t \quad [1]$$

$$\Delta\omega(t)=-\mu\beta\tanh\beta t \quad [2]$$

where A_0 is the peak B1 amplitude, μ is a phase modulation parameter (dimensionless) and β is an amplitude modulation parameter (in units of rad/s). The peak B1 amplitude must exceed the minimum threshold given by Eq. [3] to fulfill the adiabatic passage condition:

$$A_0 \gg \frac{\sqrt{\mu}\beta}{\gamma} \quad [3]$$

The spectral bandwidth (BW) of the hyperbolic secant pulse can be obtained from the product of the amplitude modulation and phase modulation parameters: μβ. By modifying either or both of these parameters, the BW of the HS pulse can be altered. The conventional LGE sequence uses a HS inversion pulse with μ = 5 and β = 670 rad/s, which yields a BW of 1.1 kHz. We designed a wideband HS inversion pulse using μ=16 and β = 750 rad/s, which yielded a BW of 3.8 kHz. We implemented this pulse with a peak B1 amplitude A_0 = 19 μT, which is higher than the minimum required 11.2 μT according to Eq. [3], and produces an

inversion efficiency of 92% on resonance based on Bloch simulations. In comparison, the conventional inversion pulse uses a B1 amplitude of 12 μT, which produces an inversion efficiency of 93%.

Off-Resonance Artifacts in a 3D Sequence

In 2D and 3D MRI, the slice/slab-selective excitation process is governed by the equations:

$$z=\frac{\omega_0}{\gamma G_{SS}} \quad [4]$$

$$\Delta z=\frac{BW_{RF}}{\gamma G_{SS}} \quad [5]$$

where z is the location of the slice/slab center, Δz is the slice/slab thickness, ω_0 is the carrier frequency of the radiofrequency (RF) pulse, BW_{RF} is the spectral bandwidth of the RF pulse, G_{SS} is the slice/slab selection gradient, and γ is the Larmor constant.

The presence of an ICD gives rise to spatially varying off-resonance. As a result, the slice/slab profile is distorted as:

$$z=\frac{\omega_0+\omega_{off}(z)}{\gamma G_{SS}} \quad [6]$$

where $\omega_{off}(z)$ is the spatially varying frequency offset. So, the magnitude of distortion as a function of z location is given by:

$$\text{distortion}=\frac{\omega_{off}(z)}{\gamma G_{SS}} \quad [7]$$

Therefore, when imaging a 100 mm slab with the conventional 3D LGE, at a distance of 7 cm from an ICD (where the resonance offset is approximately 3 kHz (8)) the slab distortion would be 51.4 mm (according to Eqs. [5] and [7]; bandwidth for RF excitation pulse = 5.83 kHz in the conventional 3D LGE). A slab profile distortion as large as this can give rise to an “extended” signal void, as demonstrated in Figure 1b. This would happen because even though selective slab excitation is subject to off-resonance distortion, phase encoding along the slice direction (3D slice encoding) is not distorted by off-resonance. As a result, the slice encoding process would image regions which were not excited due to slab profile distortion. This would give rise to an extended signal void which is not caused by intravoxel dephasing alone, and consequently would be larger than that produced in a 2D image. Extended signal voids were produced in phantoms, as described in Methods and Results, and observed in an ICD patient.

The distorted slab profile can extend beyond the slab oversampling range and wrap-around along the slice encode direction and overlap onto the other side of the imaging volume. This form of a through-plane wraparound can give rise to a unique ripple artifact, because the spatial phase variation of the two overlapping regions (one within the encoded slab, and one

wraparound signal due to slice distortion) would be different due to different proximity to the ICD. The signal phases of the overlapping regions can be constructive or destructive, depending on the location, which results in spatial “ripples” with interleaved dark and bright signals in this region. The formation of these ripple artifacts is demonstrated in Figure 1c. Ripple artifacts were produced in phantoms and demonstrated in volunteers, as described in the Methods and Results sections.

Therefore, to reduce the signal void and ripple artifacts, it is necessary to minimize the slab distortion overlap. According to Eq. [7], the slab distortion is inversely proportional to the slice/slab select gradient, G_{SS}. For a given slab thickness, a higher G_{SS} can be used if the bandwidth of the RF excitation pulse is increased (Eqs. [4] and [5]). In the example of the 100 mm slab excitation, if an RF excitation pulse of bandwidth 12 kHz is used, the distortion would be reduced from 51.4 mm to 25 mm. Reduced slab distortion would also give rise to reduced signal void and reduced ripple artifacts. Thus, by increasing the RF excitation bandwidth, it should be possible to reduce the artifacts that occur in 3D imaging under strong off-resonance conditions.

The ripple artifact can also be reduced by increasing the slice-oversampling factor. This would reduce the slab distortion overlap, and consequently lead to reduced ripple artifact. However, this will lead to prolonged scan times, which can be unacceptable in a clinical setting.

Off-Resonance Artifact in 2D LGE versus 3D LGE

The extended signal void and ripple artifacts are unique to 3D MRI and do not occur in 2D imaging because the slice distortion in 2D MRI is much smaller than in 3D MRI. This is primarily because the slice in 2D MRI is typically much thinner than the slab thickness in 3D MRI; hence, the 2D slice-selection gradient is typically much stronger than the slab-selective gradient in 3D MRI. In 2D LGE, for a typical slice thickness of 8 mm and a typical RF excitation pulse BW of 2.67 kHz, a slice-select gradient of 7.83 mT/m is required. According to Eq. [7], this would produce a distortion of 9 mm under an off-resonance condition of 3 kHz. This is in sharp contrast to the large distortion produced in 3D LGE, as described in the example above. Furthermore, slice encoding is not carried out in 2D MRI, as opposed to 3D MRI. Therefore, there is no possibility of the through-plane wrap-around that was described above for 3D MRI, and hence, extended signal voids and ripple artifacts do not occur in 2D LGE. However, it is advisable to increase the excitation RF BW of 2D LGE to minimize the slice profile distortion caused by the cardiac devices.

METHODS

Excitation Pulse Modifications

The conventional RF excitation pulse used in the 3D sequence in our MRI systems was a sinc pulse apodized by a Hanning window and had a single sidelobe on either side of the central lobe. The duration and BW of this pulse was 600 μs and 5.83 kHz. For a slab thickness of 160 mm (which is the typical slab thickness used for 3D LGE of the ICD patients in this study), the conventional RF excitation pulse required a slab select gradient

0.86 mT/m. The peak B1 amplitude of the conventional RF excitation pulse was 7.57 μT for a flip angle of 20°. The new RF excitation pulse was created from the conventional pulse by modifying its bandwidth-time-product parameter in the sequence to produce a new bandwidth of 12 kHz without changing the duration. Therefore, the new RF excitation pulse was also a sinc pulse apodized by a Hanning window and had three sidelobes on either side of the central lobe. The duration and BW of the new pulse was 600 μs and 12 kHz. The peak B1 amplitude of the new RF excitation pulse was 15.66 μT for a flip angle of 20°. For a slab thickness of 160 mm, the new RF excitation pulse required a slab select gradient 1.76 mT/m. It should be noted that it was not possible to use a substantially higher slab select gradient for this slab thickness, as it would require an RF pulse with a much higher BW; however, a higher BW RF pulse would require a B1 amplitude that would exceed the hardware limit. Both the conventional and modified excitation pulses were modeled with a Bloch simulator in Matlab to study the BW. Figure 2 shows the profile of the conventional and modified RF excitation pulses.

Inversion Pulse Modifications

The narrowband and wideband adiabatic inversion pulses were modeled with a Bloch simulation in Matlab (The Mathworks, Natick, MA) to examine the RF bandwidth. The wideband inversion pulse was implemented into the conventional LGE sequence (inversion-prepared 3D spoiled gradient echo sequence) by replacing the conventional narrowband pulse. The conventional narrowband pulse was implemented with a B1 amplitude of 12 μT. The B1 amplitude of the wideband pulse was set to 19 μT to achieve an inversion efficiency similar to the conventional pulse.

Phantom Studies

Phantom studies were carried using a standard American College of Radiology (ACR) phantom, to test the effect of the wideband inversion pulse, to demonstrate the formation of extended signal void artifact and ripple artifact and to demonstrate that the modified wideband 3D LGE sequence with wideband inversion and high bandwidth excitation pulses can reduce these artifacts. An ICD was placed at a distance of 5–10 cm from the phantom and the conventional 3D LGE, the wideband 3D LGE (with wideband inversion pulse only), and the modified wideband 3D LGE (with wideband inversion and wideband excitation pulses) sequences were used to acquire 3D images (40–70 slices). Sequence parameters for phantom studies were: repetition time (TR): 3.4 ms, echo time (TE): 1.15–1.25 ms, flip angle: 20°, readout bandwidth: 1000 Hz/pixel, resolution: $1.9 \times 1.9 \times 2\ mm^3$ (no zero-filling interpolation), 35 k-space lines per RR interval, slice over-sampling: 20–33%. All phantom images were acquired in the y–z plane. A few phantom images were reformatted to the x–z plane to demonstrate the ripple artifacts. Navigator gating was switched off during phantom experiments.

In Vivo Studies

Written informed consent was obtained from all participants, and the HIPAA-compliant protocol was approved by the Institutional Review Board. All in vivo experiments in healthy volunteers and patients were conducted using a 1.5T system (Avanto, Siemens Healthcare, Erlangen, Germany). The protocol for imaging our ICD patients was designed to carefully

follow the guidelines established by the European Society of Cardiology (7) as well as the literature (3–6). In particular, the ICD was interrogated and reprogrammed as appropriate before and after the MR scan. Specific absorption rate (SAR) was closely monitored during scans to ensure that it remained below 2 W/ kg. Only patients whose rhythms were not pacemaker dependent and who had no abandoned leads were included in the study. The patients' vital signs were monitored by means of ECG, pulse oximetry and blood pressure by an advanced cardiac life support-certified nurse practitioner, who was present during the entire scan.

To demonstrate the additional benefit of the high bandwidth RF excitation pulse in 3D LGE, both the wideband 3D LGE and the modified wideband 3D LGE sequences were used to image 6 healthy volunteers, who did not receive any gadolinium contrast injection. An ICD was attached to the left shoulder of each volunteer. The inversion pulse was applied on every other heartbeat (1 inversion pulse per 2 RR intervals), and a TI of 400–500 ms was used to suppress the myocardium. The sequence was ECG-gated and respiratory-gated using navigators. Images of the left ventricle (LV) were acquired in the short axis (SHAX) orientation, as well as four-chamber long axis orientation. Sequence parameters for 3D LGE of healthy volunteers were: TR: 3.4 ms, TE: 1.5 ms, flip angle: 20°, readout bandwidth: 500 Hz/pixel, resolution: $1.9 \times 1.9 \times 1.9$ mm^3 (no zero-filling interpolation), 35 k-space lines per RR interval, slice oversampling: 23–33%, TI = 400–500 ms, matrix size: $192 \times 144 \times 48$–60. Both the wideband and the modified wideband 3D LGE sequences were used with the same sequence parameters.

LGE images were also acquired from 5 VT patients, with previously implanted ICDs, who were referred to cardiac MRI for pre-ablation evaluation. All patients were referred for cardiac MRI for clinical purposes independent of this study. Appropriate MRI safety guidelines for scanning these patients were followed, including interrogating the device before and after imaging (3–7). Patients received gadolinium contrast injection (Magnevist, 0.2 mmol per kg of body weight) approximately 15 min before LGE. The modified wideband 3D LGE images were acquired in the SHAX orientation (slice thickness = 4 mm). The wideband inversion pulse was applied on every other heartbeat (1 inversion pulse per 2 RR intervals). The recently reported wideband 2D LGE (8,9), which has been integrated into the routine clinical practice of imaging these patients at our institution, was also used to acquire a stack of SHAX slices to cover the ventricles, as well as two to four two-chamber and four-chamber long axis slices. In one patient, the conventional 3D LGE was also acquired for comparison purposes. SAR values were obtained for both 2D LGE and modified 3D LGE images from the image headers. Sequence parameters for modified wideband 3D LGE of ICD patients were: TR: 2.7–3.4 ms, TE: 1.15–1.5 ms, flip angle: 20°, readout bandwidth: 500–1000 Hz/pixel, resolution: $1.4 \times 1.4 \times 4$ mm^3 (no zero-filling interpolation), 35 k-space lines per RR interval, slice oversampling: 25–40%, TI= 250–400 ms, matrix size: $256 \times 192 \times 40$–48. Sequence parameters for the wideband 2D LGE protocol for ICD patients were: TR: 4.1 ms, TE: 1.5 ms, flip angle: 25°, readout bandwidth: 500 Hz/pixel, resolution: 1.4×1.9 mm^2 (no zero-filling interpolation), 15 k-space lines per RR interval, slice thickness = 8 mm, matrix size: 256×144 (reconstructed to 256×192), TI= 250–400 ms. 2D LGE images were acquired as a single breath-hold per slice, and a total of 10–12 slices were acquired to cover the entire left ventricle.

TI was selected for ICD patients by using a Look-Locker based TI scout sequence (24,25). The standard TI scout sequence uses a balanced steady state free precession (bSSFP) readout, which does not work well in ICD patients due to strong banding artifacts. We replaced the bSSFP readout with a spoiled gradient echo readout and added our wideband inversion pulse, which produces artifact-free TI scout images (26). TI was determined using this modified TI scout sequence in ICD patients.

Data Analysis

For the patients with ICDs, SNR of the blood-pool signal, and contrast-to-noise ratio (CNR) of the contrast difference between blood-pool and myocardium were calculated for the wideband 2D LGE and modified wideband 3D LGE images. Noise was calculated as the standard deviation of the background signal. SNR and CNR values were calculated from three mid-ventricular slice images. For the patients with ICDs, both the wideband 2D LGE images and the modified wideband 3D LGE images were scored to compare the subjective image quality using a 1–4 point scale (1 = very good, 2 = good, 3 = fair, 4 = poor). The same 1–4 point scoring system was used to compare the image quality (with a focus on image artifact) between the wideband 3D LGE and the modified wideband 3D LGE in the healthy volunteers. In addition, the presence/ absence of extended signal voids and ripple artifacts were scored in the wideband 3D LGE and modified wideband 3D LGE images in a blinded manner based on the 6 healthy volunteer data. For each volunteer data set, the blinded evaluator was presented the two 3D LGE volumes in random order, and was asked to score the image based on how severely the artifact affected the appearance of the myocardium, using a 1–4 point scale (1 = no artifact with excellent definition and clear depiction of anatomy, 2 = mild artifact with good definition such that pathology can be confidently visualized, 3 = moderate artifact with poor definition such that only gross features are evaluable, and 4 = severe artifact with nondiagnostic image). An individual final score was assigned for each type of artifact in each volunteer. The scores were compared using Wilcoxon matched-pairs signed-ranks test. These analyses were carried out using the statistical package STATA version 12.0 (College Station, TX 77845). The SNR, CNR, and SAR values of the LGE scans in healthy volunteers and ICD patients were also compared using a paired t-test. A *P*-value less than 0.05 was considered to be statistically significant.

RESULTS

Excitation Pulse and Inversion Pulse Simulations

Figure 2 shows the Bloch simulation results of the excitation pulses used in the conventional and the modified wideband 3D LGE sequences, and their corresponding transverse magnetization, which shows their bandwidth. Both excitation pulses were sinc pulses apodized by a Hanning window, and had a duration of 600 ms. The conventional (old) excitation pulse had a BW of 5.83 kHz, and consequently a single sidelobe on either side of the central lobe. The modified (new) excitation pulse had a BW of 12 kHz, and consequently 3 sidelobes on either side of the central lobe.

Bloch simulation results of the conventional and the wideband inversion pulses are shown in Figure 3. The increased BW of the wideband inversion pulse (3.8 kHz as opposed to 1.1 kHz

in the conventional inversion pulse) is clearly evident from the longitudinal magnetization plots. According to Eq. [3], the conventional inversion pulse requires a minimum peak B1 amplitude of 5.6 μT to achieve adiabatic passage. On the scanner, the conventional pulse was implemented with a peak B1 amplitude of 12 μT, which allowed it to achieve an inversion efficiency of 93%, according to the simulation (Figure 3, lower left). The wideband inversion pulse requires a minimum peak B1 amplitude of 11.2 μT to achieve adiabatic passage, according to Eq. [3]. Bloch simulations showed that a peak B1 amplitude of 11.2 mT for the wideband pulse would result in an inversion efficiency of 56%. We, therefore, implemented the wideband pulse with a peak B1 amplitude of 19 μT. This resulted in an inversion efficiency of 92%, as shown in Figure 3 (lower right).

Phantom Studies

The wideband IR pulse was successfully implemented in the wideband 3D LGE and it was able to eliminate the hyperintensity artifact caused by the ICD, as we expected based on recent wideband 2D LGE work (8,9). Figure 4 shows the results of a phantom experiment to demonstrate the inversion efficiency of the wideband inversion pulse, and the effect of its increased bandwidth. A TI of 110 ms was used to null the contents of the phantom, which appear dark in the upper regions of the phantom, far from the ICD in Figure 4b. However, due to strong off-resonance, the regions of the phantom close the ICD were not nullified and consequently has a strong signal. In Figure 4c, due to the use of the wideband inversion pulse, a larger portion of the phantom is nullified.

Additional artifacts were discovered in the wideband 3D LGE images, which were not present in the corresponding wideband 2D LGE images. These artifacts included increased signal voids (Fig. 5) and a ripple artifact (Fig. 6). These artifacts are attributable to the slab distortion due to off-resonance that can occur in the conventional 3D LGE images, as described in the Theory section and illustrated schematically in Figure 1.

Figure 5 shows phantom images at the same slice location using the previously reported wideband 2D LGE (left), the wideband 3D LGE (middle), and the modified wideband 3D LGE (right). All parameters except bandwidth of excitation pulses were identical in the two 3D LGE images. The extended signal void in the phantom was clearly reduced in the modified wideband 3D LGE sequence, which indicates that the higher bandwidth of the excitation pulse can reduce the extended signal void artifact. The signal void in the 3D LGE images were not caused by intravoxel dephasing alone because the 2D image has much smaller signal void. Distortion of the slice profile in the 2D image is evident as the square grid fades toward the bottom of the image.

In Figure 6, the ripple-like artifacts were produced by the slab distortion, when the distorted slab wraps around and overlaps the image on the other side. The difference in spatial phase variation produces an interference-like pattern, resulting in the dark and bright ripples shown in Figures 6d,g. These ripple artifacts were reduced by increasing the bandwidth of the excitation pulse and consequently reducing slab distortion wrap-around shown in Figures 6e – h.

In Vivo Studies

The effectiveness of the wideband IR pulse in eliminating hyperintensity artifacts in an ICD patient is demonstrated in Figure 7. The left column shows a conventional 3D LGE image acquired at three slice locations. Hyperintensity artifacts obscured most of the myocardium, and nulled myocardium is not visible. The right column shows the same images slices acquired using the wideband 3D LGE. All hyperintensity artifacts were eliminated, and nulled myocardium is clearly visible. Regions of scar are also visible at the anterior and posterolateral walls of the left ventricle (arrows).

Figure 8 shows the effectiveness of the modified wideband 3D LGE sequence in removing the ripple artifacts. These images were acquired from two healthy volunteers, without contrast, on whom an ICD was attached near the left shoulder. With the wideband 3D LGE sequence, ripple artifacts were produced in the LV (Fig. 8a). However, using the modified wideband 3D LGE sequence, these ripple artifacts were significantly reduced. In Figure 8c, the ICD caused both ripple artifacts and extended signal void in the LV when using the wideband 3D LGE and both artifacts were removed using the modified wideband 3D LGE (Fig. 8d). In these images, TI = 400 ms; images were acquired across the whole myocardium in the four-chamber horizontal long axis (HLA) orientation. Note these are non-contrast scans; hence, the signal-to-noise was not the same as what one would achieve post-contrast. Nevertheless, the benefit of the modified wideband 3D LGE was clearly shown without the need for contrast agents. All parameters except the bandwidth of the excitation pulse were identical for both sequences.

Figure 9 shows a comparison between the wideband 2D LGE images and the modified wideband 3D LGE in two ICD patients. The 2D images had a resolution of 1.4 × 1.9 × 8 mm, while the 3D images had a resolution of 1.4 × 1.4 × 4 mm. The 3D images have superior image quality and improved spatial coverage of the LV, and provide improved information on the scar transmurality. Figure 9a compares the SHAX images of both the 2D and 3D LGE images at several slice locations. Figures 9b,c shows the four-chamber, HLA view which was reformatted from the 2D and 3D images in A. Figure 9b was created by stacking the 2D images to form the volume and reformatted. The large slice thickness and slice mis-registration is clearly evident in the 2D reformatted image. In the 3D image, mis-registration is avoided and the slice resolution was 100% higher than 2D LGE. Figures 9d–f shows a similar comparison on a different ICD patient.

Data Analysis

In the five ICD patients, the SNR and CNR was 37614 and 30612, respectively, for the modified wideband 3D LGE, which was not significantly different from the wideband 2D LGE (31617 and 24615 for SNR and CNR, respectively) (P=0.36 for the SNR comparison and P = 0.28 for the CNR comparison). The median and interquartile range (IQR) (expressed as median[IQR]) of the image quality scores were 1.5[1.25] for the wideband 2D LGE and 2.5[1.25] for the modified wideband 3D LGE. The difference was not statistically significant (P = 0.58). In the six healthy volunteers, the image quality score of the modified wideband 3D LGE showed a trend of being improved over the wideband 3D LGE (2.25[1.5] for the modified wideband 3D LGE versus 3[0.75] for the wideband 3D LGE, P = 0.05).

The ripple artifact score of the modified wideband 3D LGE was significantly better than the wideband 3D LGE (2[0.75] versus 3[0], $P<0.05$). The extended signal void artifact score was 2[0.75] for the wideband 3D LGE and 2[1.5] for the modified wideband 3D LGE. The difference was not statistically significant ($P = 0.56$).

SAR values remained well below the FDA limit of 2 W/kg in all volunteer and ICD patient scans for the wideband 2D LGE, wideband 3D LGE and the modified wideband 3D LGE sequences. In the ICD patient scans, the SAR was 0.10 ±0.01 W/kg (range: 0.09 to 0.11) for the wideband 2D LGE and 0.42 ±0.12 W/kg (range: 0.22–0.52 W/kg) for the modified wideband 3D LGE, and the difference was statistically significant ($P<0.05$), which is expected because the modified wideband 3D LGE sequence is more SAR intensive. In the healthy volunteer scans, SAR for the wideband 3D LGE was 0.43 ± 0.06 W/kg (range: 0.36 to 0.52 W/kg), and it was significantly higher at 0.51 ± 0.05 W/kg for the modified wideband 3D LGE ($P<0.05$). This increase is most likely due to the fact that the modified wideband 3D LGE sequence used an RF excitation pulse with a higher BW, and consequently a higher peak B1 amplitude, and same duration.

DISCUSSION

LGE MRI is an important technique for assessing myocardial viability and fibrosis (27). For patients undergoing catheter ablation of VT, the assessment of scar transmurality, size and location provided by LGE MRI enables accurate identification of the arrhythmogenic substrate leading to more effective selection of sites for ablation. This has the potential to decrease procedure time and increase success rate for ablation procedures. The current clinical standard of LGE is a 2D sequence with a typical resolution of (1.4 × 1.9 × 6–8 mm^3). While this is often considered “high” in many cardiac MRI applications, it may not be sufficient to provide the detailed information about scar morphology and transmurality that would be valuable for RF ablation procedures, and it may not be sufficient for the identification of small focal lesions. It is not feasible to simply carry out 2D LGE MRI with an increased resolution, because this would give rise to images with suboptimal SNR. High resolution LGE images are feasible using a 3D LGE sequence. However, there has been no prior report studying the feasibility and image artifacts of 3D LGE in the presence of strong off-resonance caused by cardiac devices.

The results of our study suggest that, with appropriate modifications to RF pulse design, diagnostic 3D LGE MR images can be acquired successfully in patients with implanted cardiac devices. We implemented a modified wideband 3D LGE cardiac MRI protocol for patients with implanted devices, which included replacing the conventional inversion pulse with a wideband (3.8 kHz) inversion pulse. The increased bandwidth of the inversion pulse is essential for avoiding hyperintensity artifacts in the myocardium, which are produced by the strong off-resonance induced by an ICD (8,9). If any region of the myocardium experiences off-resonance greater than 1 kHz, then the spins in those regions will not be nulled by the conventional inversion pulse, and will register in the image as hyperintensity artifacts; off-resonance in the myocardium of ICD patients can be as high as 6 kHz (8). The second modification to the 3D LGE sequence presented here was increasing the bandwidth of the excitation pulse. The increased distortion in 3D imaging when compared with 2D

imaging can give rise to extended signal voids and ripple artifacts, which are typically not seen in 2D imaging. We demonstrated that by increasing the RF excitation pulse bandwidth, these signal voids and ripple artifacts could be significantly reduced or removed. While extended signal voids and ripple artifacts do not appear in 2D LGE, slice distortion in 2D MRI does take place in the presence of cardiac devices, and this distortion can be reduced in 2D LGE MRI by increasing the excitation RF pulse BW, similar to our proposed technique for the modified wideband 3D LGE.

Several metal artifact reduction techniques have been previously reported (16,17,21,28). Multispectral imaging approaches, such as MAVRIC or SEMAC (16,17), have been shown to greatly reduce artifacts caused by metallic implants. However, these types of techniques typically require prolonged acquisitions because either the image acquisition is repeated several times in different spectral bands or additional phase-encoding is applied in 2D slice direction; this could be a major problem for 3D LGE MRI because the need for ECG gating would further lengthen image acquisition time. For example, a multi-spectral 3D LGE sequence could require up to 30–45 min of scan time, which would be clinically impractical. For our myocardial scar imaging application, because the device is typically at a distance of 5–10 cm away from the heart, there is no need to reduce metal artifacts at immediate proximity of the device. Therefore, although increasing the bandwidth of the excitation RF pulse might not be as effective as multispectral methods, it was sufficient for our application and it does not prolong the acquisition time. Furthermore, the effect of strong device-related off-resonance on the inversion pulse has rarely been studied in previous metal artifact reduction techniques, and our wideband inversion pulse clearly addresses this issue. Overall, the device-caused problem in 3D LGE is somewhat unique in comparison with the general problem caused by metallic implants and our modified wideband 3D LGE approach is inspired by but different from existing metal artifact reduction methods (16,17,21,28,29).

The ripple artifact is generated under somewhat unique conditions. It only happens when there are both slab aliasing and phase accumulation within the TE. As we demonstrate in the phantom figure (Fig. 6), the ripple artifacts occur only when there is overlap of the distorted region with another part of the image (Figures 6d,g). As shown in the figure, when there is no overlap, there is no ripple artifact (Fig. 6a). In cases where there is only phase accumulation within TE, but no slab aliasing, signal void will exist where there is significant intra-voxel dephasing. However, in such cases, the signal loss should not have the striped spatial patterns as shown in Figure 6, but would be simply a solid signal void area. It should be noted that the ripple artifacts might be altogether eliminated in the conventional 3D LGE sequence, simply by increasing the slice oversampling factor. The slab distortion would then project into the oversampling space, and would not be wrapped around to produce any ripple artifacts. However, the slice oversampling may need to be as high as 100% of the slab thickness, and this would lead to prolonged scan times. In addition, increasing the slice oversampling factor will not affect the extended signal voids in any way.

One alternative option for eliminating both extended signal void and ripple artifacts would be to use nonselective excitation for 3D LGE. In nonselective excitation, no slice/slab selection gradient is used, and the RF pulse excites all tissue within reach of the coil assuming the nonselective excitation has sufficiently high spectral bandwidth. Because both

the extended signal voids and ripple artifacts are caused by distortion of the slab selection profile, nonselective excitation would be an ideal approach for eliminating both of these artifacts. However, nonselective excitation would lead to prolonged scan times, because phase encoding and slice encoding would have to be large enough to prevent any aliasing artifacts. Nonetheless, nonselective excitation is an approach that needs to be explored carefully, especially in the context of accelerated imaging, where the scan times may be feasible in a clinical setting.

Limitations

The main limitation of our study is that our modifications to the excitation pulse can reduce the slab distortion artifacts, but may not completely eliminate them. The degree of distortion reduction depends on the magnitude of the slab select gradient: the higher the slab select gradient, the greater the reduction in slab profile distortion. In this study, we designed the modified wideband 3D LGE protocol for imaging the whole left ventricle. Consequently, we had to use a slab thickness of at least 10 cm. For such a large slab thickness, the highest slab select gradient we could use was 2.82 mT/m, which required that we use an RF excitation pulse with BW of 12 kHz and a B1 amplitude of 15.7 μT. It was not possible to further reduce the distortions by further increasing the slab select gradient, because this would require an RF excitation pulse with a higher BW and a higher B1 amplitude which may exceed the hardware limit. Furthermore, our modifications to the 3D LGE sequence address only the slab profile distortion artifacts (through-plane artifacts), but do not address in-plane artifacts, such as signal void due to intravoxel dephasing and readout distortion due to frequency encode process. A spin-echo sequence or a sequence with ultrashort TE may be able to correct for strong intravoxel dephasing signal voids, and a high receiver bandwidth and/or view angle tilting (20) may reduce the readout distortion.

ACKNOWLEDGMENTS

Grant sponsor: National Institutes of Health; Grant number: 1R21 HL118533.

The authors thank Grace H. Kim, PhD, for help with statistical analyses.

REFERENCES

1. Roger VL, Go AS, Lloyd-Jones DM, et al. Heart disease and stroke statistics-2012 update: a report from the American Heart Association. Circulation. 2012; 125:e2–e220. [PubMed: 22179539]
2. Kalin R, Stanton MS. Current clinical issues for MRI scanning of pacemaker and defibrillator patients. Pacing Clin Electrophysiol. 2005; 28:326–328. [PubMed: 15826268]
3. Nazarian S, Hansford R, Roguin A, et al. A prospective evaluation of a protocol for magnetic resonance imaging of patients with implanted cardiac devices. Ann Intern Med. 2011; 155:415–424. [PubMed: 21969340]
4. Nazarian S, Roguin A, Zviman MM, et al. Clinical utility and safety of a protocol for noncardiac and cardiac magnetic resonance imaging of patients with permanent pacemakers and implantable-cardioverter defibrillators at 1.5 tesla. Circulation. 2006; 114:1277–1284. [PubMed: 16966586]
5. Cohen JD, Costa HS, Russo RJ. Determining the risks of magnetic resonance imaging at 1.5 tesla for patients with pacemakers and implantable cardioverter defibrillators. Am J Cardiol. 2012; 110:1631–1636. [PubMed: 22921995]
6. Nazarian S, Halperin HR. How to perform magnetic resonance imaging on patients with implantable cardiac arrhythmia devices. Heart Rhythm. 2009; 6:138–143. [PubMed: 19121814]

7. Roguin A, Schwitter J, Vahlhaus C, Lombardi M, Brugada J, Vardas P, Auricchio A, Priori S, Sommer T. Magnetic resonance imaging in individuals with cardiovascular implantable electronic devices. Euro-pace. 2008; 10:336–346.
8. Rashid S, Rapacchi S, Vaseghi M, Tung R, Shivkumar K, Finn JP, Hu P. Improved late gadolinium enhancement MR imaging for patients with implanted cardiac devices. Radiology. 2014; 270:269–274. [PubMed: 24086074]
9. Stevens SM, Tung R, Rashid S, et al. Device artifact reduction for magnetic resonance imaging of patients with implantable cardioverter-defibrillators and ventricular tachycardia: late gadolinium enhancement correlation with electroanatomic mapping. Heart Rhythm. 2014; 11:289–298. [PubMed: 24140812]
10. Rashid, S.; Plotnik, A.; Litt, H.; Han, Y.; Rapacchi, S.; Tung, R.; Shivkumar, K.; Finn, JP.; Hu, P. Abstracts of the 17th Annual SCMR Scientific Sessions. New Orleans, Louisiana, USA: 2014. Artifact reduction with a wideband late gadolinium enhancement (LGE) MRI technique for patients with implanted cardiac devices: a two-center study. Abstract 44
11. Akcakaya M, Rayatzadeh H, Basha TA, Hong SN, Chan RH, Kissinger KV, Hauser TH, Josephson ME, Manning WJ, Nezafat R. Accelerated late gadolinium enhancement cardiac MR imaging with isotropic spatial resolution using compressed sensing: initial experience. Radiology. 2012; 264:691–699. [PubMed: 22820734]
12. Kino A, Zuehlsdorff S, Sheehan JJ, Weale PJ, Carroll TJ, Jerecic R, Carr JC. Three-dimensional phase-sensitive inversion-recovery turbo FLASH sequence for the evaluation of left ventricular myocardial scar. AJR Am J Roentgenol. 2009; 193:W381–W388. [PubMed: 19843715]
13. Peukert D, Laule M, Taupitz M, Kaufels N, Hamm B, Dewey M. 3D and 2D delayed-enhancement magnetic resonance imaging for detection of myocardial infarction: preclinical and clinical results. Acad Radiol. 2007; 14:788–794. [PubMed: 17574129]
14. Taclas JE, Nezafat R, Wylie JV, Josephson ME, Hsing J, Manning WJ, Peters DC. Relationship between intended sites of RF ablation and post-procedural scar in AF patients, using late gadolinium enhancement cardiovascular magnetic resonance. Heart Rhythm. 2010; 7:489–496. [PubMed: 20122877]
15. Koch KM, Hargreaves BA, Pauly KB, Chen W, Gold GE, King KF. Magnetic resonance imaging near metal implants. J Magn Reson Imaging. 2010; 32:773–787. [PubMed: 20882607]
16. Koch KM, Lorbiecki JE, Hinks RS, King KF. A multispectral three-dimensional acquisition technique for imaging near metal implants. Magn Reson Med. 2009; 61:381–390. [PubMed: 19165901]
17. Lu W, Pauly KB, Gold GE, Pauly JM, Hargreaves BA. SEMAC: slice encoding for metal artifact correction in MRI. Magn Reson Med. 2009; 62:66–76. [PubMed: 19267347]
18. Lu W, Pauly KB, Gold GE, Pauly JM, Hargreaves BA. Slice encoding for metal artifact correction with noise reduction. Magn Reson Med. 2011; 65:1352–1357. [PubMed: 21287596]
19. Butts K, Pauly JM, Gold GE. Reduction of blurring in view angle tilting MRI. Magn Reson Med. 2005; 53:418–424. [PubMed: 15678535]
20. Cho ZH, Kim DJ, Kim YK. Total inhomogeneity correction including chemical shifts and susceptibility by view angle tilting. Med Phys. 1988; 15:7–11. [PubMed: 3352554]
21. Koch KM, Brau AC, Chen W, Gold GE, Hargreaves BA, Koff M, McKinnon GC, Potter HG, King KF. Imaging near metal with a MAVRIC-SEMAC hybrid. Magn Reson Med. 2011; 65:71–82. [PubMed: 20981709]
22. Tannus A, Garwood M. Adiabatic pulses. NMR Biomed. 1997; 10:423–434. [PubMed: 9542739]
23. Bernstein, MA.; King, KF.; Zhou, ZJ. Handbook of MRI pulse sequences. Boston: Academic Press; 2004. xxii,1017
24. Gupta A, Lee VS, Chung YC, Babb JS, Simonetti OP. Myocardial infarction: optimization of inversion times at delayed contrast-enhanced MR imaging. Radiology. 2004; 233:921–926. [PubMed: 15516607]
25. Look DC, Locker DR. Time saving in measurement of NMR and EPR relaxation times. Rev Sci Instrm. 1970; 41:250–251.
26. Rashid, S.; Tung, R.; Shivkumar, K.; Finn, JP.; Hu, P. Abstracts of the 17th Annual SCMR Scientific Sessions. New Orleans, Louisiana, USA: 2014. Improved inverstion time (TI) scout

sequence for late gadolinium enhancement mri of patients with implantable cardiac devices. Abstract 146

27. Simonetti OP, Kim RJ, Fieno DS, Hillenbrand HB, Wu E, Bundy JM, Finn JP, Judd RM. An improved MR imaging technique for the visualization of myocardial infarction. Radiology. 2001; 218:215–223. [PubMed: 11152805]
28. den Harder JC, van Yperen GH, Blume UA, Bos C. Ripple artifact reduction using slice overlap in slice encoding for metal artifact correction. Magn Reson Med. 2014
29. Kolind SH, MacKay AL, Munk PL, Xiang QS. Quantitative evaluation of metal artifact reduction techniques. J Magn Reson Imaging. 2004; 20:487–495. [PubMed: 15332257]

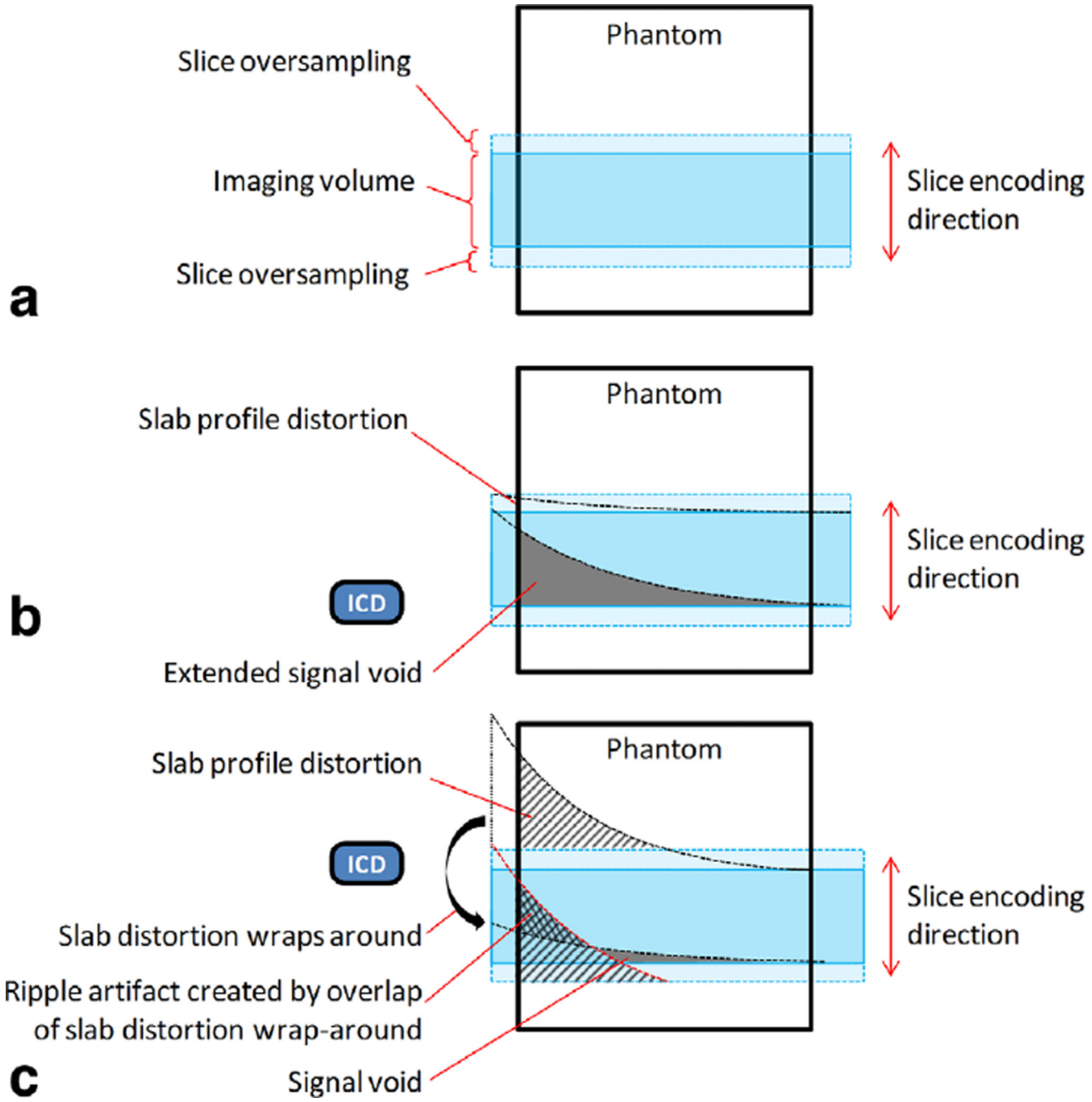

FIG. 1.

Diagram demonstrating the formation of the extended signal void and the ripple artifact due to off-resonance produced by an ICD in a 3D selective volume excitation in a phantom. **a:** Setup of the imaging volume. The 3D slice encoding direction here is top–bottom. The slice oversampling region shown here is approximately 20% of the slab thickness. **b:** When the ICD is placed near the lower boundary of the imaging volume, the RF excitation profile is distorted as shown. The distortion would be stronger at the lower boundary than the upper boundary, due to closer proximity to the ICD and consequently higher off-resonance. In the

gray zone, spins are not excited, resulting in an extended signal void. **c:** When the ICD is positioned near the upper boundary of the imaging volume, distortion of the RF excitation profile causes the spins in the region labeled “slab profile distortion” to be excited. Because this region extends beyond the slice oversampling region, it wraps around to the bottom of the imaging volume. Here, it overlaps with the imaging volume and produces ripple artifacts, because the spatial phase variation in the two overlapping regions are different (due to their different proximity to the ICD and hence different off-resonance distributions). A small signal void region is also produced at the lower edge of the imaging volume. Note: if the polarity of the slice selection gradient is reversed in B and C, the direction of the slab distortion would be reversed. The ripple artifact would then be produced in B and the extended signal void would be produced in C.

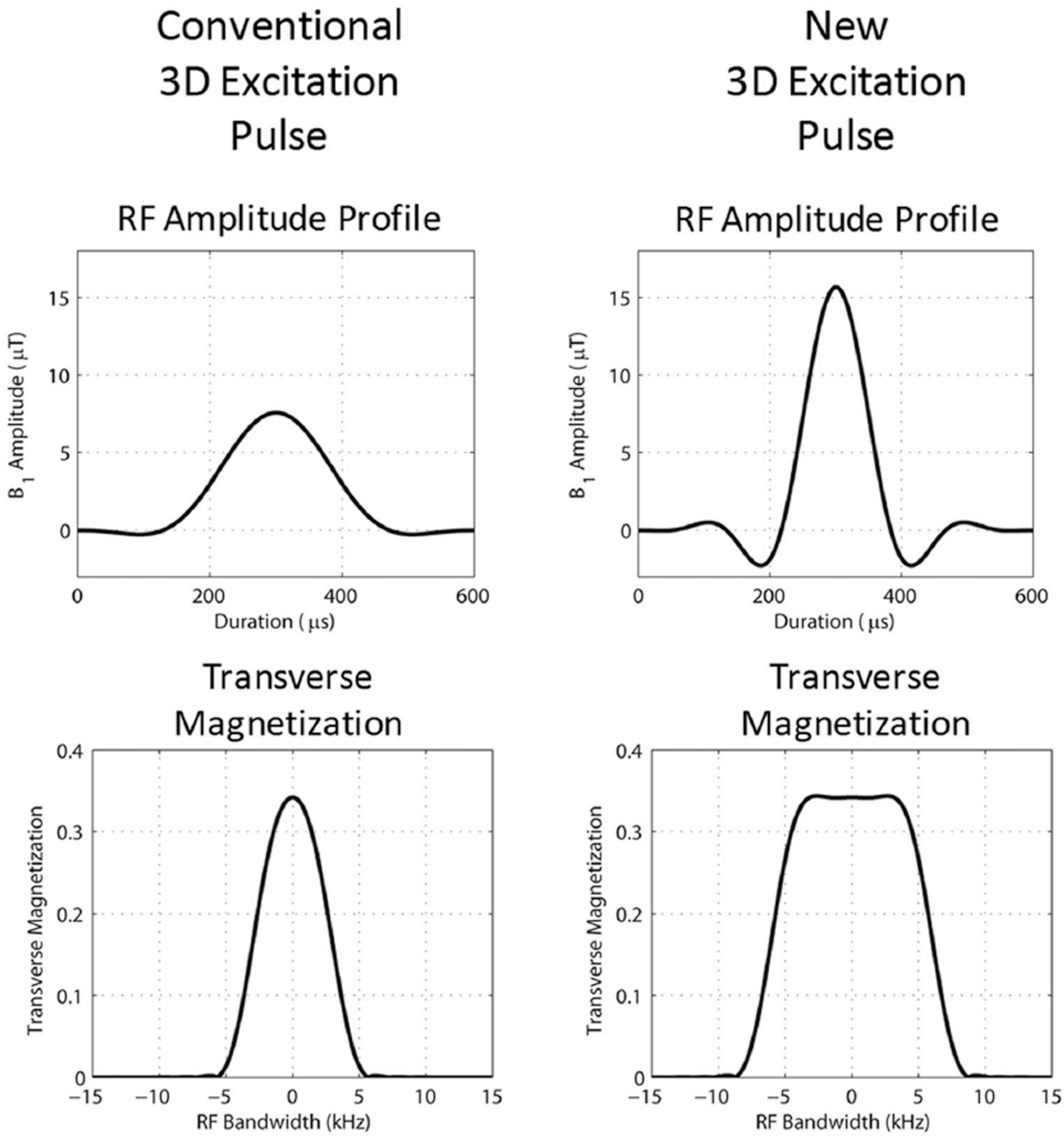

FIG. 2.

Bloch simulation results of the conventional and our modified excitation pulses in the 3D LGE sequence, showing the B1 amplitude profile and the corresponding transverse magnetization profile to demonstrate RF bandwidth. Both conventional and new RF pulses are sinc pulses apodized with a Hanning window. The conventional pulse had a bandwidth-time-product (BWT) of 3.5 and BW of 5.83 kHz, while the new pulse had a BWT of 7.2 and a BW of 12 kHz, producing a B1 profile with a narrower center lobe and higher B1 amplitude.

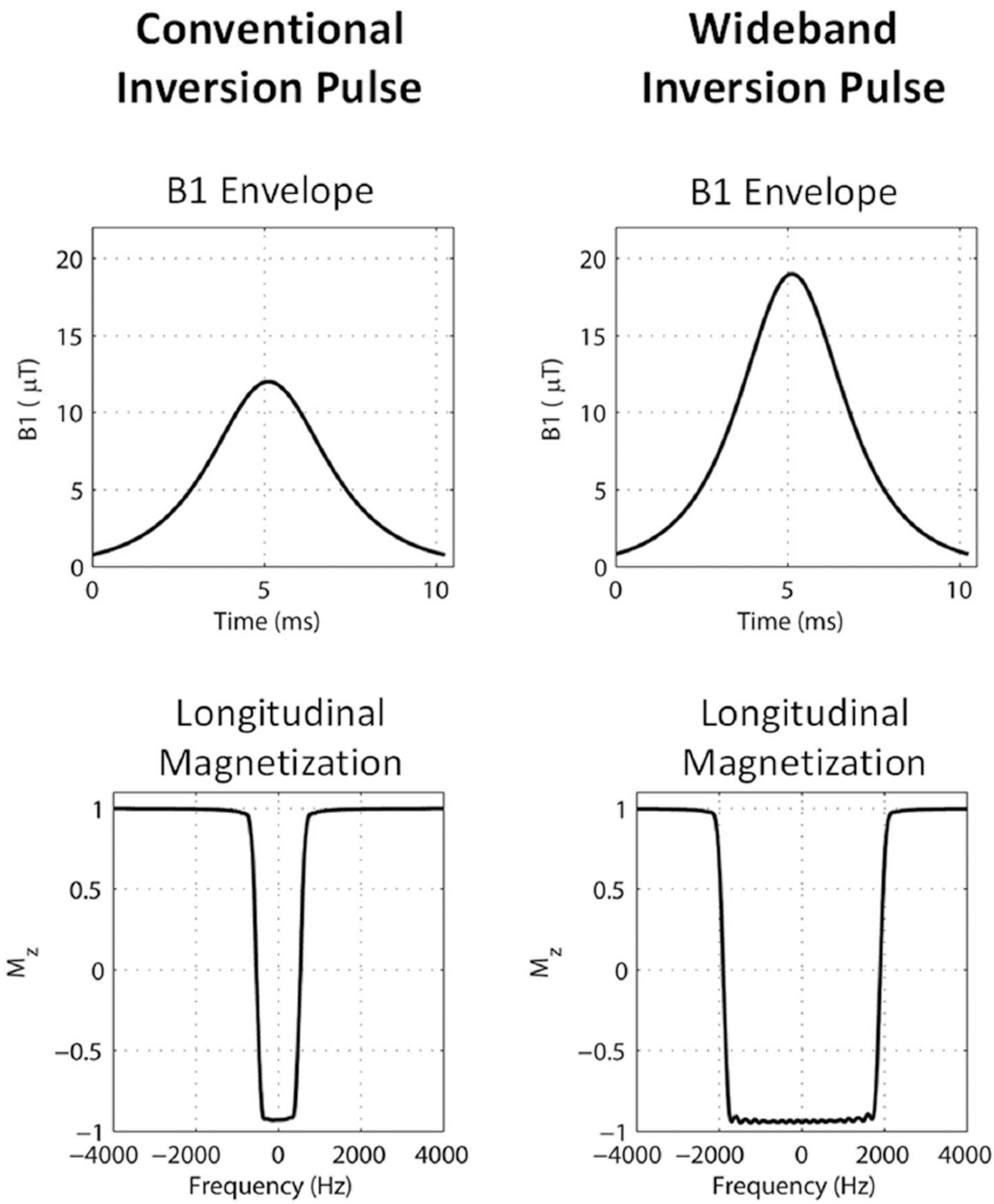

FIG. 3.

Bloch simulation results of the conventional and wideband inversion pulses in the 3D LGE sequence, showing the B1 amplitude profile and the corresponding longitudinal magnetization profile to demonstrate RF bandwidth and inversion efficiencies. Both inversion pulses were nonselective. The conventional inversion pulse had a B1 amplitude of 11.9 μT and a bandwidth of 1.1 kHz. The wideband inversion pulse had a B1 amplitude of 19 μT and a bandwidth of 3.8 kHz. The simulated inversion efficiency was 93% for the conventional pulse and 92% for the wideband pulse.

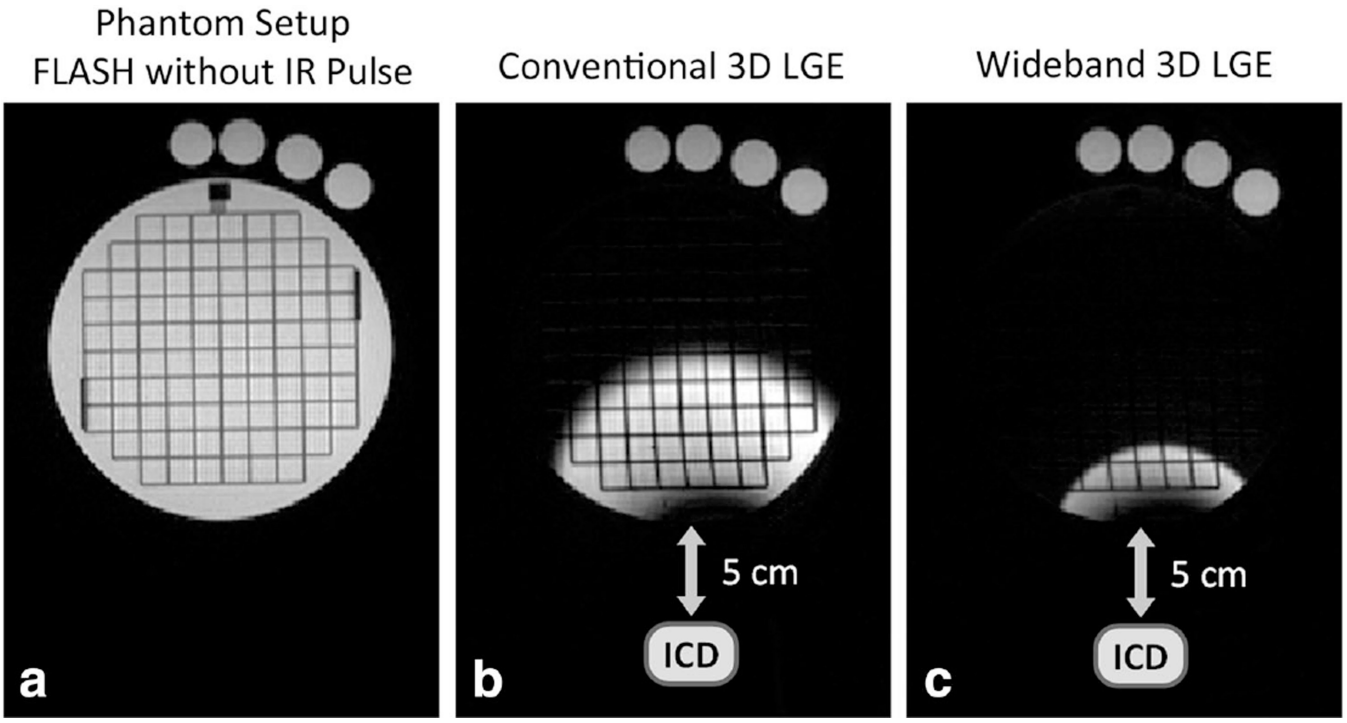

FIG. 4.

Phantom simulation showing the inversion efficiency and effect of improved bandwidth of the wideband inversion pulse. **a:** The phantom setup is shown using a FLASH sequence with no inversion pulse. An ACR phantom was used, and four test tubes containing gadolinium-doped water were placed at the upper side. The T1 of the ACR phantom contents was 160 ms, and the T1 of the test tube contents was lower than 60 ms. In B & C, the 3D LGE sequence using the conventional and wideband inversion pulse are used. TI of 110 ms was used to null the contents of the ACR phantom. An ICD was placed at 5 cm from the bottom of the phantom. **b:** Due to off-resonance induced by the ICD, the regions of the ACR phantom were not nullified in the regions close to the ICD, because these regions had off-resonance that exceeded the spectral bandwidth of the conventional inversion pulse. **c:** Due to the increased bandwidth of the wideband inversion pulse, a larger portion of the ACR phantom was nullified. The same window level was used in both B & C, which indicates that the wideband inversion pulse had similar inversion efficiency as the conventional pulse.

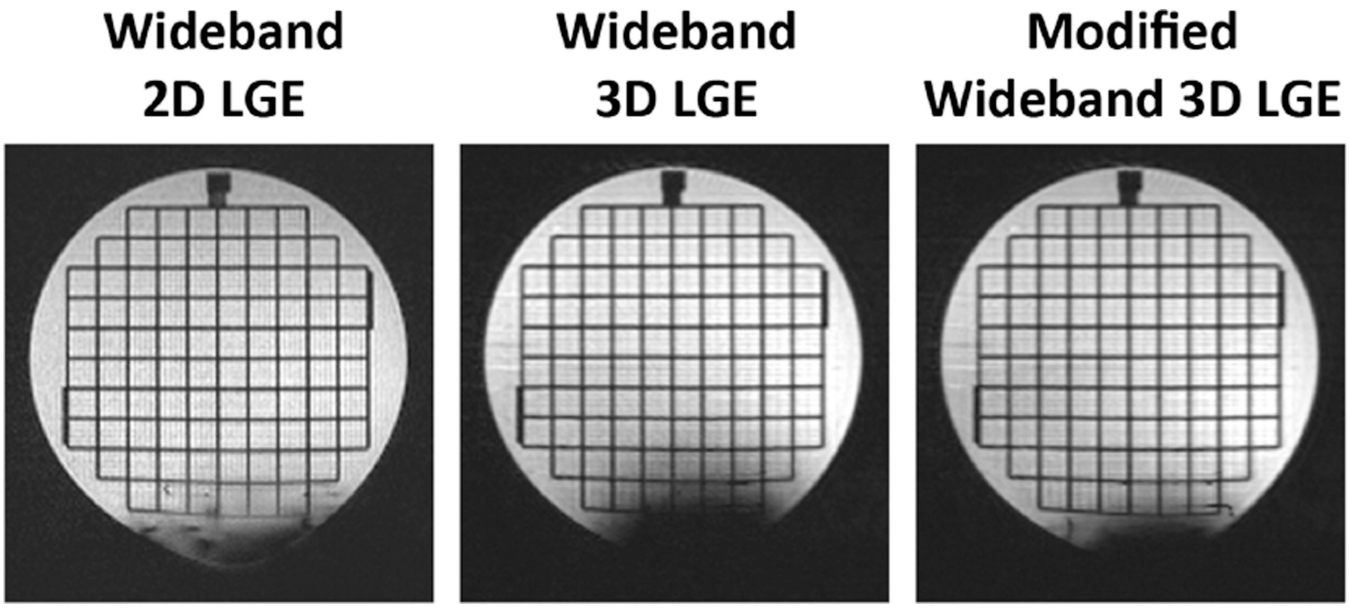

FIG. 5.

Images from an ACR phantom imaged by the conventional 3D LGE (center) and the modified 3D LGE (right) sequences. An ICD was placed at 6 cm from the phantom at the bottom. The signal void is distinctly reduced in the modified 3D LGE sequence, owing to its higher bandwidth of the excitation pulse. To demonstrate that the signal void is a consequence of slab distortion as well as intravoxel dephasing, a 2D LGE image of the same location is shown (left). The signal void in the 2D is a consequence of only intravoxel dephasing, and so it is smaller in 2D than in 3D. For these images, TE in the 2D sequence was 1.52 ms, and TE in both 3D sequences was 1.25 ms.

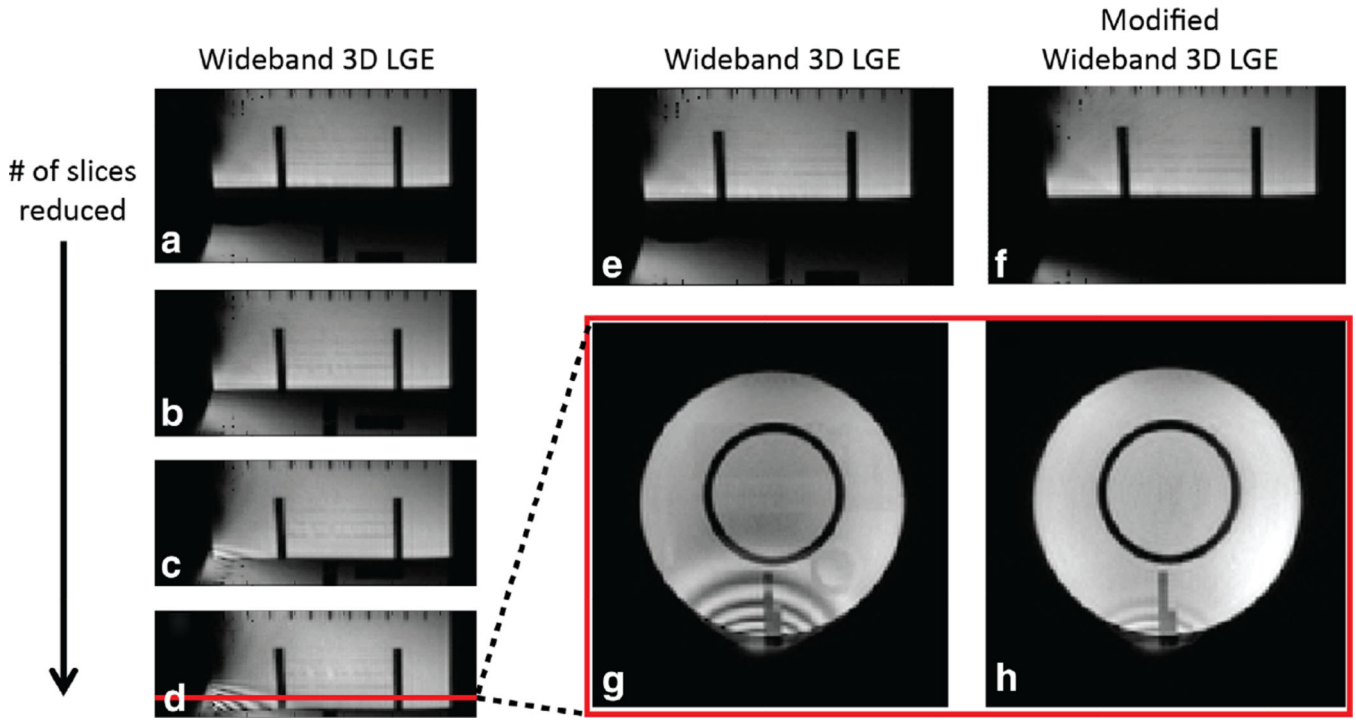

FIG. 6.

a–d: Demonstration that the ripple artifact is produced by overlap of the slab wrap-around artifact in the conventional 3D LGE sequence. These images were reformatted to the edge-view so that the slice encode direction is top-bottom. An ICD was placed 5 cm away from to the left of the phantom. In A, the aliased distorted slab profile is visible at the bottom of the image. As the slab thickness (number of slices) is progressively reduced from A to D, the distorted slab profile moves upward, until it overlaps with the bottom of the phantom, producing ripple artifacts in C and D. **e–h:** Images showing that the modified wideband 3D LGE sequence can reduce the slab distortion and overlap, consequently reducing the ripple artifacts. The large slab distortion in E is significantly reduced in F due to the increased excitation RF BW in F. In G, the image was acquired with the wideband 3D LGE (wideband inversion only), which results in significant ripple artifacts. In H, the same phantom location as G was acquired using the modified wideband 3D LGE, which results in significantly reduced slab distortion/wrap-around and hence reduced ripple artifacts. (D and G are reformatted versions of the same 3D volume).

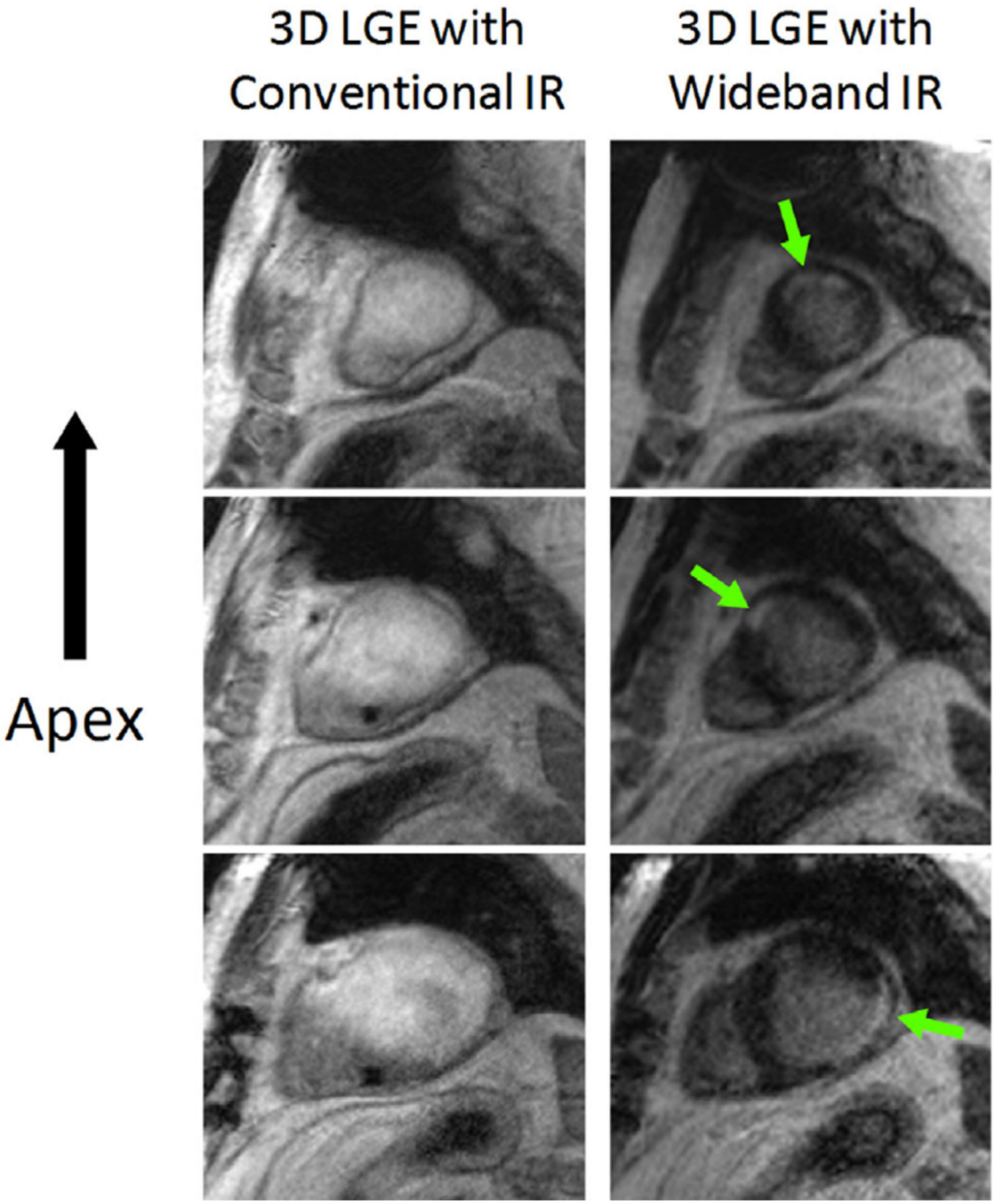

FIG. 7.

Three slices of the myocardium acquired with 3D LGE sequences using the conventional inversion pulse (left column) and wideband inversion pulse (right column) in an ICD patient. In the left column, the conventional inversion pulse with BW of 1 kHz was used; consequently hyperintensity artifacts were produced throughout most of the myocardium. In the right column, the wideband inversion pulse with 3.8 kHz BW was used, giving rise to nulling of healthy myocardium, as expected. Regions of scar tissue are visible in all 3 slices of the wideband LGE acquisition (arrows), but are obscured in the conventional inversion

pulse images. These two 3D LGE images were acquired with a thin slab (36 slices in each volume, and 1.9mm slice thickness without zero-filling interpolation). It is noted that the ripple artifacts described in this study did not appear in these images due to the use of a thinner slab acquisition.

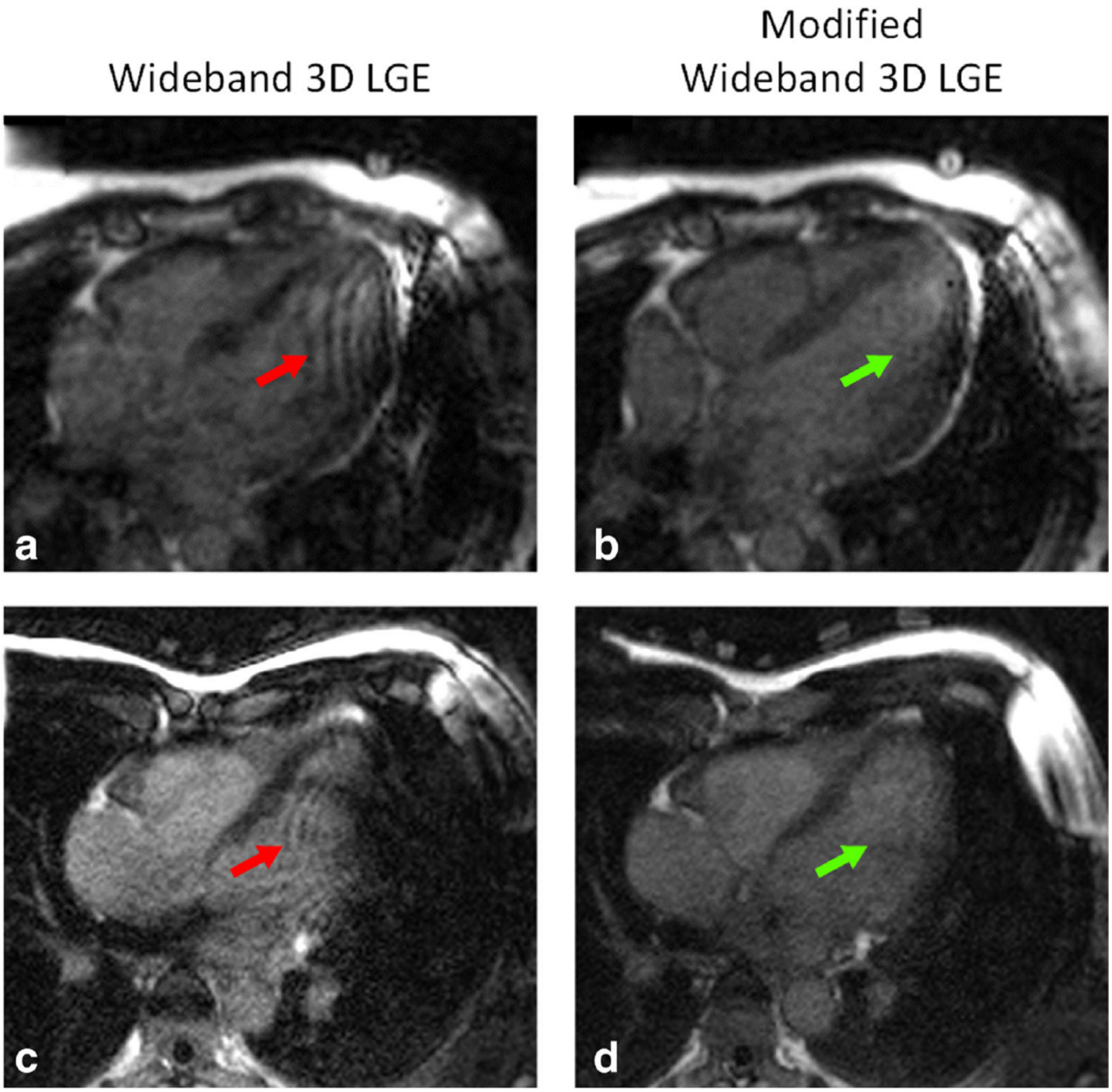

FIG. 8.

a,c: Examples of ripple artifacts and extended signal void (red arrows) in two healthy volunteers (non-contrast) acquired with the wideband 3D LGE sequence. **b,d:** Both types of artifacts are significantly reduced (green arrows) when using the modified wideband 3D LGE sequence. An ICD was placed at the left shoulder of the volunteers in all four images.

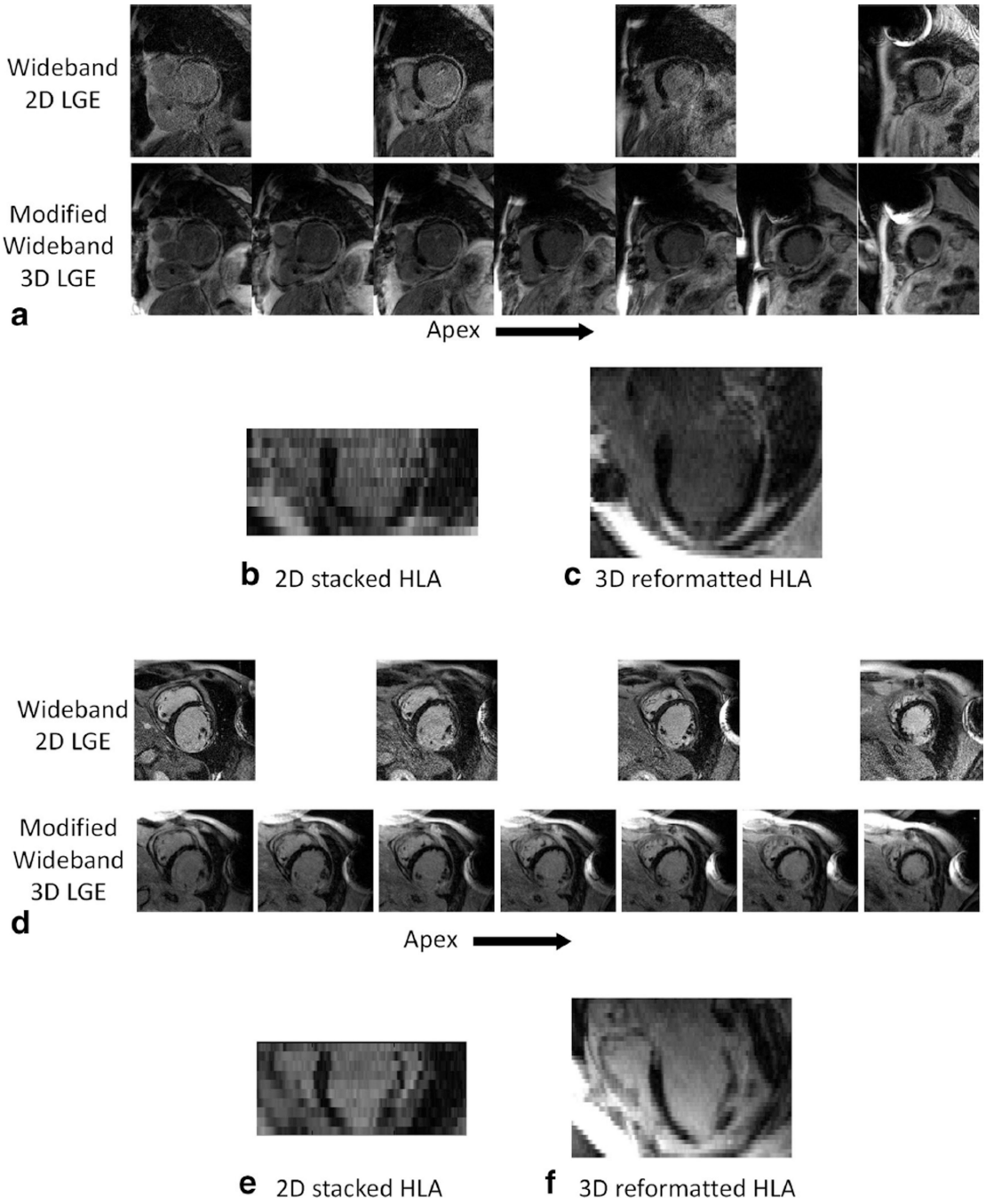

FIG. 9.

a: Comparison between the wideband 2D LGE sequence the modified wideband 3D LGE sequence at the same slice locations of the myocardium from two ICD patients who were scheduled for VT ablation. The 3D images appear less noisy and provide better coverage of the myocardium and scar regions. The ICD is located at the upper-left of the image. **b,c:** Four-chamber HLA images created from the 2D (B) and 3D (C) LGE images. In (B), the 2D LGE images were stacked to produce the volume, and reformatted to the HLA view. The large slice thickness and slice mis-registration is evident in the 2D reformatted image (B),

while the 3D volume and higher slice resolution in (C) produces a better HLA image. **d–f:** A similar comparison on a different ICD patient. Note the slices in the 2D scans were 100% thicker than the 3D scans.